Graphical Representation Of Flight Electro-Mechanical Actuators Test Data And Systems Health Monitoring Parameters Using Lissajous Patterns Enabling Automation.

Sreedhar Babu G[1,2], Sekhar A S[1] and Lingamurthy A[2]

1 Department of Mechanical Engineering, Indian Institute of Technology Madras, Chennai, Tamilnadu, 600036, India
me12d017@smail.iitm.ac.in
as_sekhar@iitm.ac.in

2 Control Systems Laboratory, Research Centre Imarat, Hyderabad ,Telangana, 500069, India
gsreedhar.rci@gov.in
almcsrci@gmail.com

ABSTRACT

Linear electromechanical actuators are popular in flight servo-actuation systems. Repertories of mandatory acceptance and health-monitoring tests result in the generation of large amounts of data. This poses challenges in handling the volumes of similar data sets by quality/systems health engineers, causing fatigue in making critical decisions. Attempt is made to ease such tasks by representing the data in a pictorial form to easily identify the parameters of interest. This study focuses on the use of Lissajous figures to pictorially represent the acceptance and condition monitoring test data the flight actuators. A graphical interpretation of acceptance test data represented by Lissajous patterns, aimed at the automation of test outcomes, is attempted. The extraction of system health indicators for mechanical faults in electromechanical linear actuators is also attempted. The results will help in developing expert systems taking advantage of current efficient pattern recognition and classification algorithms. This study focuses on easing the critical flight-worthiness clearance jobs of quality engineers and extracting system health parameters from test data represented graphically.

1. INTRODUCTION

Servo actuators are flight-critical in aerospace applications. Voluminous data is generated owing to the mandatory tests conducted in the process of ensuring flight worthiness. The costs of failures in such systems are disastrous and justify numerous performance tests and system health monitoring needs. The flight actuator tests start with qualification tests to validate the design and acceptance tests to verify the workmanship and production-related issues. Performance tests are mandated before, during, and after such tests. Tests such as environmental Stress Screening (ESS) include these performance tests to be performed before in pre-environmental tests (PREET), in-situ environmental tests (INSET), and post-environmental tests (POET)) to ensure that the unit under test (UUT) is good at each stage. Additional tests of the actuators before the final integration in the flight are conducted to eliminate storage and handling related issues. These tests consume an appreciable amount of life for such systems, particularly in the case of missile and safety-critical single-shot operation systems. In-flight data is collected throughout the service life or at periodic intervals to determine the system's health parameters. All of the above tests lead to the generation of a large amount of test data to be verified by quality engineers. These test datasets are similar, repetitive, and mandatory. Their review is flight critical, resulting in fatigue for the quality engineer. Hence, a strong need of simplifying such laborious tasks efficiently is the need of the day. In this paper, we attempt to represent the acceptance and condition monitoring data in graphical form using Lissajous figures aimed at easing the work of quality engineers and a step towards automation. Lissajous figures are suitable for graphically representing parametric equations. Lissajous figures are popular in engineering and are known to generate stationary patterns on cathode ray tubes with two mutually orthogonal inputs. They are used to represent vibrations, such as the periodic motion of the U-tongues. Technical paper (NASA, 1980) used Lissajous patterns to record the nonlinear transients of a flexible rotor by passing through three critical speeds, and used Lissajous patterns to verify the three critical speeds at three mode shapes.

https://doi.org/10.36001/IJPHM.2024.v15i2.3965

One look is worth a thousand words. It is inherently easy for humans to classify the images. With recent extensive research in the fields of biometrics, face recognition, and classification problems, many efficient, standardized algorithms for real-time use in the classification of big data sets are abundantly available, which can mimic human-like capabilities. Repetitive activities such as acceptance of servo actuators used in flight control actuation and cumbersome activities such as health monitoring of engineering systems are solid candidates to take advantage of such research. In this paper, we attempt to represent the outcomes of performance test data in graphical form to ease the quality of inspectors' jobs. Extending this technique to the extraction of system health parameters will ease and accelerate fault classification by humans and computing machines as a result of non verbal representation. Test data repositories can be used to develop expert systems leading to the supervised learning of classification algorithms, aimed at automating system health monitoring. Gurevich, Yashina and Ablameyko (2018) developed an expert system and presented the algorithms for image analysis applied to the identification of the state of retinal blood flow and morphometric analysis of the state of endothelium in the human eye cornea by combining machine learning and expertise of ophthalmology specialists based on image processing. Such expert systems are suitable for health monitoring in engineering systems. Graphical representation of test data is required to extend these types of expert systems for engineering systems health monitoring problems.

Efficient algorithms are available for graphical data classification, including character and text recognition, image segmentation, and object detection and recognition. Graphics recognition, a subfield of pattern recognition, is extensively used for complex and huge data classification with human-like abilities in image recognition. Recognition of graphical features in heterogeneous documents, such as electrical circuit diagrams, sketches, drawings, and handwritten scribbles, is current topic of research. Xiaowen and Juncheng (2021) developed algorithms to read engineering drawings, easing draftsman's laborious tasks. Such algorithms can be extended to acceptance testing if the test data can be presented graphically. Urala, Nair, Setlur, Dasgupta, Scott, Venu and Rajan (2018) presented image processing techniques for the automated analysis of phase diagrams and attempted to classify large-scale, indexable, and digitized databases of phases under different thermodynamic conditions. They were successful to isolate phase boundaries in compositions of a wide variety of materials and subsequently extract areas of the same phase. This has eased the workload for experts in material science, by training expert systems with their field knowledge. In recent years, owing to its ability to exploit the superior representation of big data and its prediction performance, deep learning (DL) has demonstrated great success in various applications of pattern recognition and artificial intelligence for data in 2D spatial image forms. A pictorial representation of the test data is the key in utilizing the outcome of such research in the system performance analysis and health monitoring needs of flight electromechanical actuators. This study focuses on representing the data in Lissajous figures generated during acceptance testing and condition monitoring of electromechanical linear actuators used in flight applications. The work is aimed at easing the quality and maintenance engineers' jobs, making such jobs more machine-learning friendly.

2. LISSAJOUS FIGURES

Lissajous figures are used in many engineering applications such as oscilloscopes. They are used to visually represent orthogonal vectors. Systems with oscillatory input and output can be represented as Lissajous figures by plotting the input vs. output.

The input is represented as

$$X(t) = Ax.sin\ (\omega x.t) \tag{1}$$

The output is represented as

$$Y(t) = Ay.sin\ (\omega y.t + \emptyset) \tag{2}$$

'X(t)' is instantaneous input to the system at time instant 't' and 'Y(t)' is instantaneous output from the system at time instant 't' in response to input X(t), 'Ax' is the amplitude of the input and 'Ay' being amplitude of the output. 'ωx' being the frequency of input and 'ωy' being the frequency of the output. '$\emptyset$' being the phase difference between input and output of a system. Lissajous figure can be obtained by plotting the data X(t) vs. Y(t) as an XY plot.

Input–output relations of oscillatory systems can be represented by various means; however, the Lissajous figure represents the data in a simpler and compact form. For an ideal servo system, the Lissajous figure will be a straight line with 45^o slope, representing the output following the input in phase without altering the amplitude. However, a real system acts as a low-pass filter and smears the input signal based on system parameters and load disturbances. Performance tests are conducted on systems to arrive at their performances in terms of transfer functions in both time and frequency domains. Generally, time-domain tests provide static performance parameters, and frequency-domain tests provide a better understanding of the dynamic performance parameters. Frequency-domain tests are popular for oscillatory systems.

The most important frequency domain performance parameters of a system are the gain and phase bandwidths. They are acquired from frequency response tests where the system is commanded with varying input frequencies, and the output from the system is recorded. The input and output are compared, and the frequency at which the half-power

point occurs is used to arrive at the gain bandwidth, and the frequency at 90^o phase lag occurs is used to arrive at the phase bandwidth. In this study, attempts are made to acquire this vital information from the Lissajous figures of the system input and output.

In linear servo systems, the frequencies of the input and output will be closer, resulting in a Lissajous figure with a single lobe. The dynamics of load and disturbances beyond the capability of the system will slightly alter the output frequency, resulting in a reduced frequency of the output relative to the input frequency. It is easy to identify such instants from the Lissajous figure because of the drastic change in its shape, as Lissajous figures are sensitive to frequency. Hence, it is more convenient for an operator or system to detect such changes readily from test data if represented as a Lissajous figure.

The amplitude ratio Ax/Ay used to obtain the gain bandwidth is represented by the slope of the Lissajous figure. It represents the gain graph of the frequency response plot in a pictorial form. An ideal servo is expected to generate a Lissajous figure as a straight line with a slope of 45^0, representing X(t) = Y(t) for all input frequencies. In reality, all physical systems have limited bandwidth, and the band of frequencies in which the system's output follows the input. The Lissajous figure of such systems will start at 45^0 slope for lower frequencies and will gradually rotate towards the 0^0 slope (abscissa) as the input frequency increases and settles at the 0^0 slope for further higher input frequencies compared to the system amplitude bandwidth.

The phase angle ∅ is used to arrive at the phase bandwidth. The phase angle is the angle at which the output of the system lags behind the input. In Lissajous figure, it is represented by the aspect ratio, that is, the ratio of the width to height of the Lissajous figure. Phase angle ∅ =0 produces Lissajous figure as a straight line (0 height, infinite aspect ratio) and the phase lag of 90^o transforms the Lissajous figure into a perfect circle (unity aspect ratio). Any non-zero phase angle (∅), in between 0 and 90^o produces an ellipse with aspect ratio (major axis / minor axis) proportional to the phase lag.

Armughan H., Sufi T.G. and Abdul Q.K (2016) used the Parks vector Lissajous curve as simplified technique to perform system health monitoring of three-phase induction motors using motor current signature analysis (MCSA) by checking the deviation in circularity of Park's vector Lissajous curve. This eliminated the need for high computational frequency analysis, which is generally used to obtain similar information. This method is used for stationary operation of induction motors without intelligent servo control systems.

Qing B., Dingguo S. and Jian L. (2019) conducted experiments and used Lissajous figures to correct the Hall effect sensors in permanent magnet synchronous motors as a solution to the problem of amplitude imbalance and phase offset of the linear Hall sensor output signal of servo systems. Park's transformation was used as an effective tool to detect broken bars in asynchronous motors, even at the incipient stage by Avoci M.U, Carratu. M., Pietrosanto A., Paciello V., and Lay-Ekuakille (2020). The experiment was carried out, and the Lissajous figure was applied in the case of broken bars. An increase in ellipse thickness was clearly observed in the fault cases. This is clearly demonstrated by the harmonics excited by faults. They established that the rotor broken-bar cases can easily be detected by monitoring the rise in the Lissajous ellipse thickness, confirming the utility of Lissajous figures for systems health monitoring needs.

Chenguo Y., Zhongyong Z., Yan M., Chengxiang L, Yifan L. and Guochao Q. (2015) proposed an online monitoring method for winding deformations based on the Lissajous graphical analysis of the voltage and current for power transformers that directly affect the safe operation of power grids. A load normalization method is proposed to distinguish winding deformations with different degrees and locations to solve the problem using the fact that the Lissajous diagrams change as the load varies. The study confirmed the advantages of low data rates and their use for machine learning by cloud computing. Lissajous figures were used for the extraction of electrical fault signatures in electromechanical systems. The system under study is an electro mechanical linear actuator used to maneuver the aerospace vehicles run by a brushless direct current (BLDC) motor. Techniques discussed are attempted to be extended to acceptance testing and identifying mechanical faults in the system in this study.

2.1. Lissajous figure representation of linear servo systems

The electromechanical actuators (EMA) used in flight control applications follow the properties of linearity and time invariance during their maximum portion of operational life, and for simplicity, they can be represented as linear time invariant (LTI) systems. The dynamic response of such a system is an important parameter. Loads at which the system is operating (FL) compared to its designed load (FC) and the frequency (ωx) of the input command compared to their bandwidth frequency (ωn) will decide how good can perform and follow the commanded positions. The bandwidth (ωn) of such systems is represented by two important parameters in the frequency domain: amplitude ratio and phase lag. The system bandwidth is commonly defined for such systems as the input frequency at which the system output lags by 90^o (90^o phase lag) or the input frequency at which the-3 dB point (half-power point) occurs. Lissajous patterns can be used to readily arrive at these important parameters for such systems. Lissajous patterns can be obtained by the superposition of two orthogonal harmonic signals

representing the input and output of the system. Owing to their inherent properties, linear servo systems fall in the specific category of LTI systems with nearly the same frequency at the input and output, resulting in a single-lobe Lissajous figure. Attenuation in the amplitude of the output changes the slope of the Lissajous figure. The phase lag between the input and the output alters the aspect ratio of the Lissajous figure.

Servo systems operate faithfully till the input frequency ωx < ωn.

The input is represented as

$$X(t) = Ax.sin(\omega x.t) \quad (3)$$

'Ax' being amplitude of input signal and

'ωx' being frequency of input signal

The output is represented as

$$Y(t) = Ay.sin(\omega y.t + \emptyset) \quad (4)$$

'Ay' being amplitude of output signal, 'ωy' being frequency of output signal and ∅ being the phase lag between output and input signals.

LTI systems pose no rules for the values in Eq. (3) and Eq. (4), but for the linear servos in their operational limits, owing to the physical limitations imposed:

$|Ax| \cong |Ay|$ and $0 \leq \emptyset \leq 180$ (For stability of operation)

and $\omega x \cong \omega y$

Additionally, for the electro mechanical actuators (EMA) used in this study,

$|Ax| \geq |Ay|$, as system gain is tuned to near critical damping with no overshoot, and operated at frequencies < ωn

$0 \leq \emptyset \leq 100$; as the input velocity is band limited to ensure operation at maximum power,

$\omega x \cong \omega y$ as servo actuators are practically operated within their bandwidth and, EMAs induce phase lag (negative ∅) because physical systems are causal and contribute to delay only.

The shape of the Lissajous figure from the input and output is mathematically represented in Eq. (3) and Eq. (4), as follows:

$$\frac{x(t)}{Ax} = sin\,(\omega x.t) \Rightarrow \cos \omega x.t = \sqrt{1 - (\frac{x(t)}{Ax})^2}$$

$$\frac{y(t)}{Ay} = \frac{x(t)}{Ax}cos\,\emptyset + \sqrt{1 - (\frac{x(t)}{Ax})^2} \times sin\,\emptyset$$

$$\frac{y(t)^2}{Ay^2} = \frac{x(t)^2}{Ax^2}(cos^2\emptyset) + (1 - (\frac{x(t)}{Ax})^2) \times sin^2\emptyset \quad (5)$$

The Lissajous figure of the EMA is generally an ellipse with a major axis along the X=Y line and can fall into any one of the following cases considering practical constraints.

Case 1: FL << FC and ωx << ωn

At negligible loads (FL) and very low-frequency inputs (ωx) compared to the load capability (FC) and bandwidth (ωn) of the EMA. The output frequency is close to the input frequency ωx=ωy and The output follows the input without any phase lag (∅ = 0) or attenuation (Ax=Ay).

Substituting above in (5)

$$y(t) = x(t) \quad (6)$$

results in a straight line with slope of 45° from abscissa.

Case 2: FL < FC and ωx << ωn

At loading (FL) is the fraction of the designed load capacity (FC) and low-frequency inputs (ωx) compared with the bandwidth (ωn) of the EMA.

The output follows input without any phase lag (∅ = 0) and amplitude of the output is attenuated slightly, but near unity magnitude attenuation (Ax ≅< Ay)

Substituting above in (5)

$$y(t) <\cong x(t) \quad (7)$$

results in an equation of a straight line with slope < 45°

Case 3: FL >> FC and for any ωx

At loads much greater than the capability of the EMA, the system will be stalled with no output, resulting in the X-axis figure.

$$y(t) = 0 \quad (8)$$

Case 4: FL ≤ FC and ωx ≅ ωn (general case of operation).

At loads and input frequency within the capability of EMA, the output and input are 90° apart (∅=90°), Substituting above in (5)

$$\frac{x(t)^2}{Ax^2} + \frac{y(t)^2}{Ay^2} = 1 \quad (9)$$

results in an ellipse with a major axis parallel to X axis.

Case 5: FL ~ FC and ωx = ωn

Hypothetical case of loads (FL) at bandwidth frequency of EMA, within its load capacity (FC). The output and input are in 90° phase (∅=90°) and unity attenuation, (Ax=Ay), Substituting above in (5)

$$x(t)^2 + y(t)^2 = Ax^2 = Ay^2 \quad (10)$$

results in a circle with radius 'Ax = Ay'.

From the above, it can be concluded that the frequency response parameters of the EMA system can be obtained graphically from the Lissajous figures. The slope of the Lissajous figure represents the gain bandwidth, which is a function of the attenuation (amplitude ratio). The slope of the Lissajous figure starts at 45^o for unit attenuation for low-frequency inputs and gradually becomes zero (x-axis) at higher frequencies ($\omega x >> \omega n$). The width of the figure starts diminishing at higher frequencies and the system stops responding to much higher frequencies relative to its bandwidth, resulting in a zero-width figure with a slope of zero. The first instant of zero slope with a finite width of the Lissajous figure of the frequency response test data represents the gain bandwidth (-3 dB frequency)

The phase bandwidth is represented by the phase lag and can be represented as the aspect ratio (ratio of the major axis to the minor axis) of the Lissajous figure. The width of the Lissajous figure (minor axis of the ellipse) is increased with an increase in the phase lag. It increases till 90^o phase and transforms into a circle representing the phase bandwidth (90^o phase frequency) and subsequently starts reducing again as the input frequency further increases.

The response of the EMA system is complex based on its system parameters, input dynamics, and other unwanted inputs such as load disturbances and noise. However, all of them manifest as standard frequency response test outcomes in terms of phase bandwidth and gain bandwidths, which can also be obtained from the Lissajous figures. By recording the input and output data and representing it as a Lissajous figure, we can obtain the gain bandwidth from the slope and phase bandwidth from the aspect ratio of the Lissajous figure.

3. APPLYING LISSAJOUS FIGURES TO FLIGHT ELECTRO MECHANICAL ACTUATORS TEST DATA

The typical performance of an actuator in actual flight is shown in Figure1. The in-flight performance of EMA is generally a qualitative comparison of its input and output. The input to the actuator is generally termed a command, that is, the desired position of the EMA, and the output of the EMA is generally termed as feedback, that is, the actual position achieved by EMA.

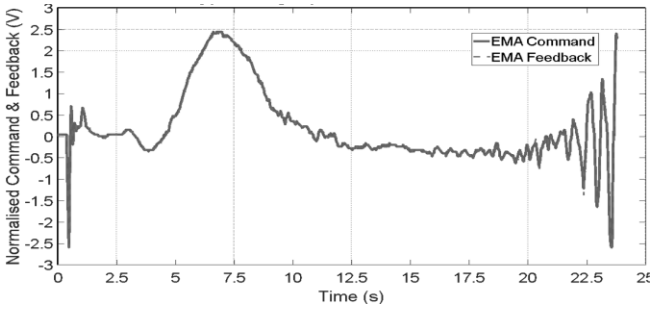

Figure 1: Command and feedback of a typical flight EMA

The plot depicts the performance of a typical actuator in a small portion of its operational envelope during an actual flight. By visual examination of the plot in Figure 1, only a qualitative conclusion can be made that, the actuator followed the command, but did not provide any quantitative measure. Most of the post-flight analyses stop here unless any specific deviation in data or flight is observed. To obtain a better insight into the same data in Figure 1, the Lissajous pattern representation of the same data is shown in Figure 2.

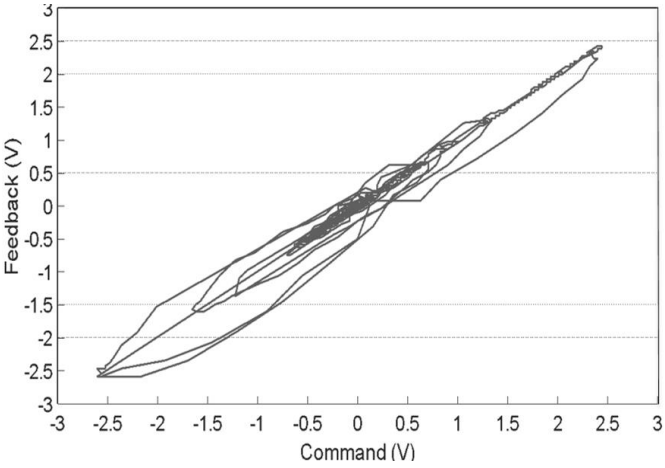

Figure 2: Lissajous figure of typical in flight EMA command and feedback data

Figure.2, provides direct insight into the flight data. The slope of the figure provides the amplitude ratio, that is, a measure of the command attenuation. The data spread (standard deviation) provides a quantitative measure of the faithfulness of the actuator to the command (nonlinearity). The width of the figure provides the maximum phase lag, which can be used to arrive at the maximum input frequency demanded during flight. In addition, careful examination of Figure 2 reveals that EMA is more linear in extending the stroke (+ve) compared to retraction (-ve). The data in the positive stroke are spread on one side to the mean line stating that the load is always opposing, but in the case of a negative stroke, data are spread on both sides of the mean line, depicting the aerodynamic loads acting in both aiding and opposing fashion.

This type of information can be visually depicted from the Lissajous representation of the flight EMA data. Large datasets can be created and used to train machine-learning algorithms in the long run. The use of Lissajous representation of flight EMA data for the automation of acceptance testing and systems health monitoring applications is discussed in subsequent sections.

3.1. Lissajous figures for acceptance tests

Flight actuators undergo a tremendous amount of testing to ensure their flight worthiness. Performance tests are

necessary to ensure that the actuator meets all operational objectives. Typical performance tests conducted were step response, frequency response, endurance, sine cycling, threshold, null bias, nonlinearity, low amplitude low frequency test, and high amplitude low frequency test. Environmental tests were conducted to ensure satisfactory performance of the actuators in their actual working environment. MIL-STD standards mandate environmental tests, such as High Temperature, Low Temperature, Bump, Endurance, High Altitude, Acceleration, Shock, Vibration, Thermal Shock and Tropical Exposure, based on the operating envelope of the EMAs. In addition, they include tests for electromagnetic interference (EMI), electromagnetic compatibility (EMC), and electrostatic discharge.

Performance tests must be conducted before and after each of the above environmental tests to ensure that the test has no adverse effects on the unit under test (UUT) and that it is healthy before, during, and after the test. EMA must perform consistently in all of the above tests.

The data generated is small in some of the performance tests, such as step response, and the acceptance criterion is straightforward, such as meeting the specified speed, overshoot, and settling times. However, in some cases, such as in endurance tests, the data is huge, and the inspector has to look for anomalies in similar looking large data sets. In the case of frequency response tests, even the data interpretation is not straightforward, and costly equipment, such as a frequency response analyzer, is needed to assess the outcome of the test. The following sections elaborate on the Lissajous pattern representation of the tests, generating huge amounts of data such as endurance and frequency response tests. Typical tests generating large data conducted on flight actuators, the current method of interpreting the data, its Lissajous representation, and the advantage of the Lissajous representation in simplifying acceptance testing are elaborated in subsequent sections.

3.1.1. Endurance tests

Endurance Test: Endurance tests were performed to ensure the performance of the system subjected to a large number of cycles. For the flight actuators, a sinusoidal command is applied, and the response is recorded. The test is conducted for each actuator at predetermined load steps and varying strokes. Typical specifications of the endurance test cases include 500 cycles at full load- quarter stroke, 500 cycles at half load - half stroke, 500 cycles at quarter load-75% stroke, and 500 cycles at no-load and full stroke.

During the endurance tests, the position command, position feedback, velocity feedback, and motor current are recorded. The acceptance criteria for the UUT to pass the test were as follows:

i) There should be no distortion in the waveforms.

ii) There should be no abnormal physical motion and

iii) No inadvertent disturbance in the velocity feedback & current waveforms.

The above is a qualitative judgement, and a quality inspector needs to thoroughly review the whole data. The endurance test setup is shown in Figure 3. The unit under test (UUT) is assembled on a hydraulic test bench capable of applying a predetermined load with a Hydraulic Loading System (HLS). The test bench had one fixed end with a load cell to record the force exerted on the UUT. There will be a provision to adjust the maximum stroke allowed on the UUT. The hydraulic loading system can load the UUT by applying a differential pressure across the load cylinder. The UUT is commanded for the necessary stroke, and the loading system is set to the specified load.

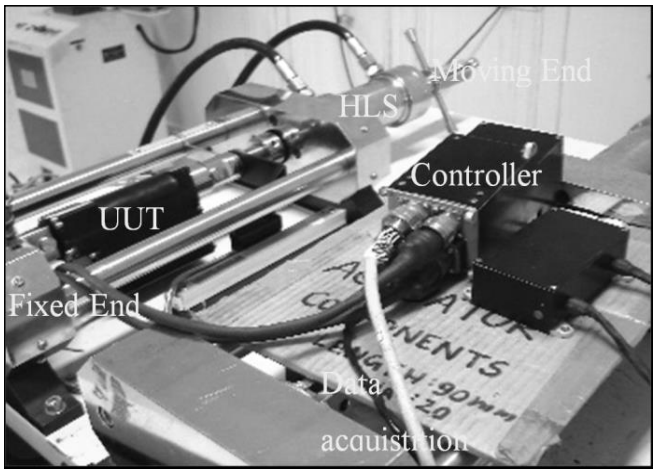

Figure 3: Endurance test setup for EMA

The test is conducted, and all data is recorded. After the test, the data is carefully verified by the quality inspector for the UUT position feedback with the command. A portion of the data recorded during one of the endurance tests is shown in Figure 4.

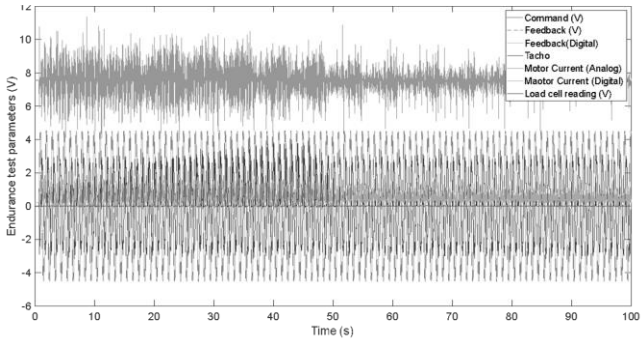

Figure 4: Data recorded during the actuator endurance test

Owing to the number of loads and cycles involved, these tests resulted in large amounts of data. Currently, data verification is performed conventionally by carefully looking into the endurance test data visually by the quality

inspector for clearing the actuator. As large numbers of actuators are produced, the data to be handled will be large. Interpretation of these test results will lead to fatigue in the test inspector, as all the plots look similar. Automated checks are currently not in force owing to safety considerations. A typical test data used to clear the actuator in the endurance test is shown in Figure 5. The actuator will be cleared in the case of no observations. If anomalies any are observed, the remaining parameters, such as the tachometer, motor current, and load cell data, are critically examined to determine the outcome of the test.

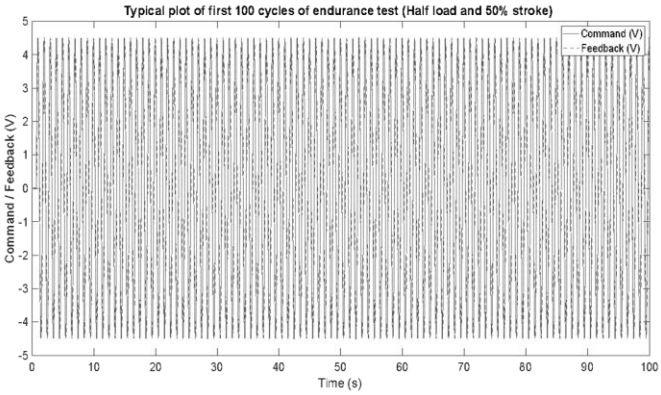

Figure 5: Typical endurance test data of actuators for acceptance

3.1.1.1 Lissajous representation of endurance test data

Lissajous figures are useful in simplifying the acceptance test outcome. Figure 5 shows the endurance test data for a healthy actuator provided to a quality engineer. Figure 6 shows the proposed representation in the form of subplots with healthy and fault-induced actuator test data. To emphasize this, each figure is provided with three subplots. The Lissajous figure (input vs. output) is shown at the top portion. The conventional plots used, input data (input vs. time) and output data (output vs. time), are shown at the bottom potion of Figure 6. It is difficult to depict the fault information of minor faults, which are more probable during acceptance tests. To elaborate on this, a 1V command at 1 Hz was applied to a Healthy EMA, as shown in Figure 6(a), which is a smooth ellipse with inclination and width based on the operating conditions. The Lissajous figure of the same EMA with a 0.1 mm dead band fault introduced in Figure 6(b) changed the Lissajous figure to a two-lobbed figure. EMA with 0.1 mm Backlash fault clipped the Lissajous figure at the extreme ends, as shown in Figure 6(c). And the same EMA with saturation of 0.9 mm introduced by dead stops has resulted in a Lissajous figure shown in Figure 6(d) with clipped extremes with extended horizontal line beyond saturation value (0.9 mm). Figure 5 and Figure 6 (a), both of which represent the same test, show that it is easier to identify anomalies during the endurance test in the case of the Lissajous figure in comparison with standard plot of endurance test data.

Hence, The study confirms the interest in Lissajous figures usage, that various faults smear the Lissajous figure in a detectable manner relatable to the fault. Hence, machine learning methods such as classifiers can be trained on large amounts of data and used to develop fault identification expert systems.

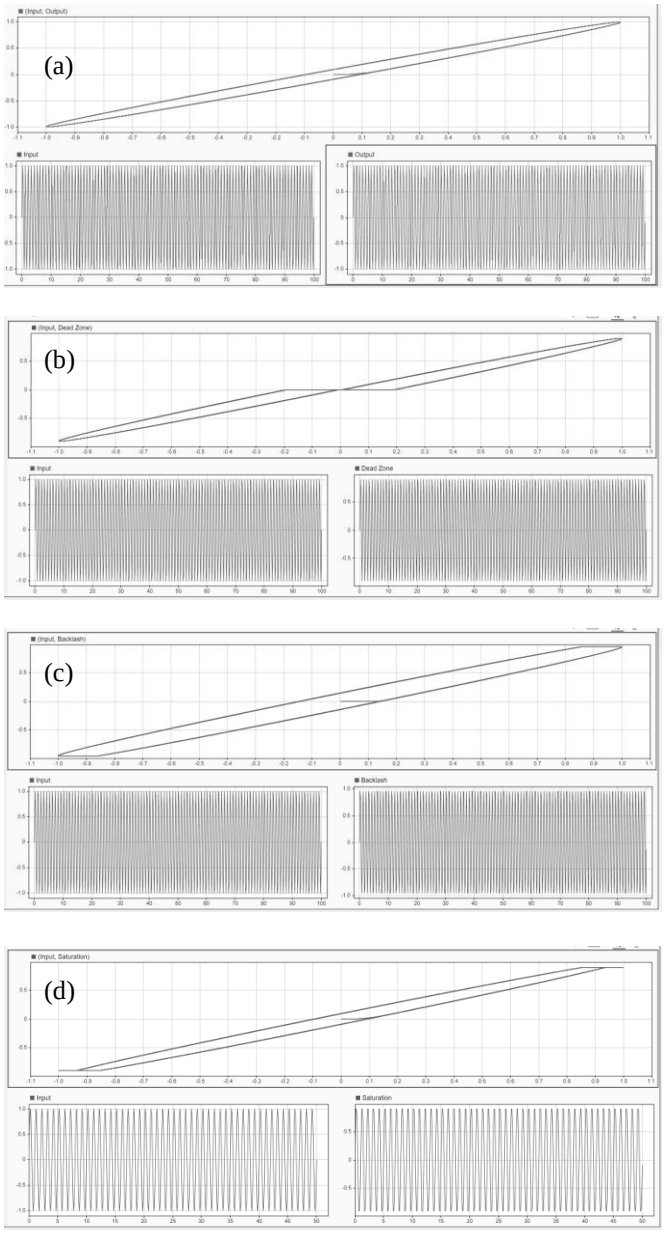

Figure 6: Lissajous figure representation of faults in endurance test data. a) Healthy, b) Deadband c) Backlash d) Saturation

In the case of Lissajous figures, all the test data is overlapped, and a faithful operation automatically acts as a reference background, making deviations easily observable.

As the endurance test is used as a pass fail criterion, the Lissajous representation plot provides simplified picture of the test data resulting in less effort to identify anomalies.

3.1.2. Frequency Response test

The most important design specification for flight control actuators is bandwidth. Frequency response test is most popular for determining bandwidth of servo actuators. Bandwidth is defined as the input frequency band in which the actuator performs faithfully. Actuator bandwidth is determined as the lowest input frequency at which the half-power point (-3 dB) occurs, or the 90^o phase lag between the input and output occurs. EMAs are typically low-pass filters; hence, they are capable of following the input from zero frequency (DC) till their bandwidth frequency.

The frequency response test is conducted by commanding the actuator with an input frequency sweep at 10% of the full-scale amplitude starting from 0 to frequency range of interest. The test is conducted using a frequency response analyzer (FRA). It generates the predetermined frequency sweeps and commands the actuators accordingly. FRA records the response from the actuator during the test. After the test, the FRA fits the response of the system to standard harmonics, Compares with input at each frequency, calculates and lists the phase and gain values in the frequency range of the test. The actuator in this study is operated at a unit amplitude (1Vp-p = 0.707 Vrms) in frequency range of 20 to 1 Hz in steps of 1 Hz with two dwell cycles at each frequency.

The frequency at phase shift of -90° is measured to determine the phase bandwidth, and the frequency at -3 dB gain is measured to represent the gain bandwidth. The input and output data in the time domain of a typical frequency-response test are shown in Figure 7. The system output initially deviated from the reference input and gradually improved and followed low-frequency commands. The data must be processed using a frequency response analyzer or post-processed to arrive at the test outcome.

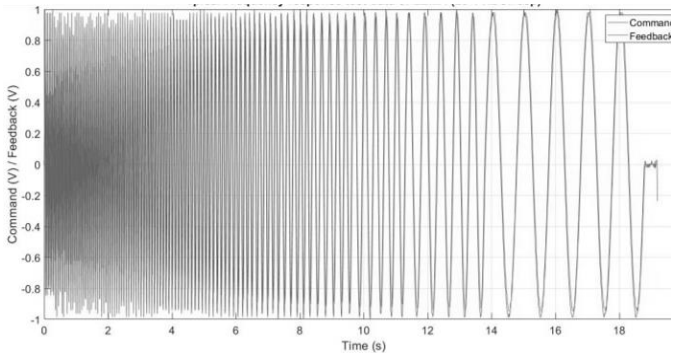

Figure 7: Time domain data of frequency response test

The results of the test in Figure 7 were obtained using a frequency response analyzer, Solartron 1250 E, in terms of the phase and gain values plotted in Figure 8. From the plots, it is evident that the EMA under test has a 90^o phase lag at 15 Hz and a half power point (-3 dB) at 16 Hz, resulting in a system bandwidth of 15 Hz.

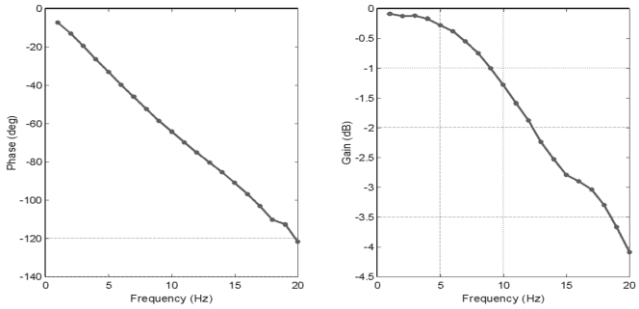

Figure 8: Phase and gain plots of typical frequency response test.

3.1.2.1 Lissajous representation of Frequency response test data

An attempt is made to take advantage of the Lissajous figures to extract results of frequency response test data. The Lissajous figure of the frequency response test presented in Figure 8 is shown in Figure 9. The actual test data will have a large amount of sensor noise and acquisition system parameters embedded in the data, and an attempt is made to generate the same data mathematically from the actuator model presented by Bhasker et al., (2015). The Lissajous figures are generated similar to the actual test conditions, and the methodology worked out to extract test outcome with ease. The same method was applied to the actual test data, and conclusions were drawn based on the comparisons. The Lissajous figure of the frequency response test of the EMA is shown in Figure 9.

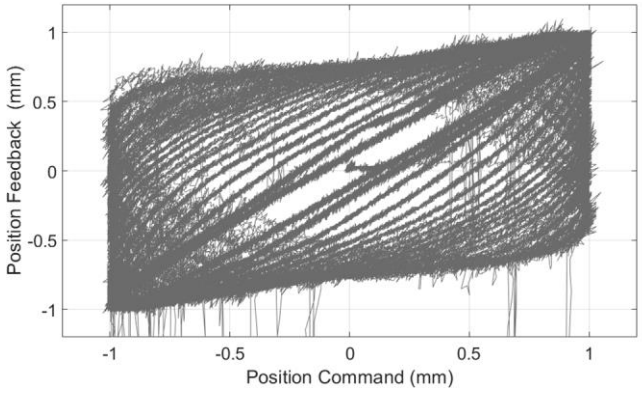

Figure 9: Frequency response test data of a healthy EMA in no load condition

The Lissajous figure of actuator (An causal LTI system) will form an ellipse lobe for each input frequency with major axis ‘a’ and minor axis ‘b. ’ The aspect ratio of the lobe is ∞ for low frequencies and decreases to 1 at the natural frequency and again increases as input frequency increases.

In the test data, the innermost ellipse in the Lissajous figure corresponds to an input frequency of 1 Hz. As the input command frequency increases from 1 to 20 Hz, the major axis of the ellipse representing the Lissajous figure rotates towards the abscissa and becomes inflated, decreasing the aspect ratio (a/b). The widest ellipse represents the 20 Hz Lissajous figure, which has the maximum attenuation and lag between the actuator input and output. Hisham Al-Khazali, and Mohamad Askari, (2012) presented a broad view of the current techniques in Lissajous curves for rotating machinery. They used an oscilloscopic rotor rig and proposed the use of Lissajous figures for rotating shafts, gears, and pumps. Similar method is worked out for servo.

The half-power point (-3 dB point) defines the gain bandwidth and the 90º phase lag defines the phase bandwidth. The same information can be inferred from the Lissajous figure. The input frequency at which the Lissajous ellipse becomes horizontal represents the gain bandwidth; at half power, the amplitude gain will be 1/√2, and the corresponding angle of the bandwidth, and Ax=Ay, represents the 90º phase lag between the input and output. As in all cases of testing flight actuators, the major axis lies between 0 and 90º, and the phase difference can be obtained from the formula $\emptyset = \frac{y}{x}$), corresponding to $\emptyset = \frac{1}{\sqrt{2}}$ = 45º. The frequency corresponding to the horizontal Lissajous figure represents actuator bandwidth. To explain this, the mathematical model of the actuator developed by Bhaskar M.R, Asish Dutta, Sreedhar Babu, Venugopal D, and A K Chattopadhyay, (2015) is used, and Lissajous figures arrived for various input frequencies, as shown in Figure 10.

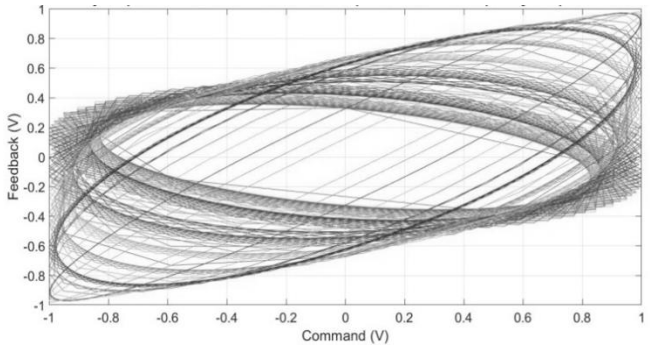

Figure 10: Command vs feedback of frequency response of EMA model

For better visibility, only a set of frequencies (1,5,10,15 and 20 Hz) was chosen for comparison with the experimental data and are shown in Figure 11. The Lissajous figure of the actual frequency response test is shown in Figure 9. The command is the unit displacement with the frequency linearly decreasing from20 Hz to 1 Hz, with five dwelling cycles at each frequency. The bandwidth of the EMA in the test was 15-17 Hz (for both the-3 dB gain and 90º phase). This can be interpreted from the horizontal Lissajous loop.

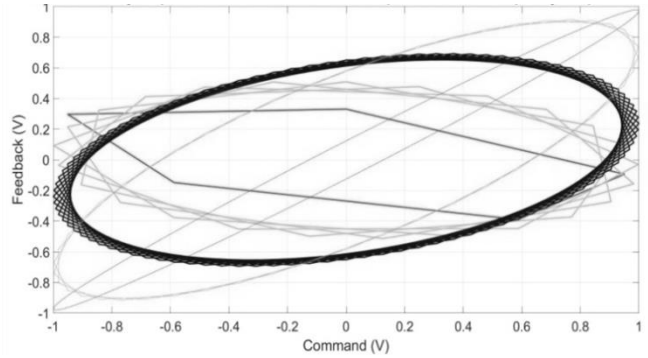

Figure 11: Lissajous figures of model data at Selected frequencies

The extracted data at the frequencies selected in the above section from the actual frequency response test data is shown in Figure 12.

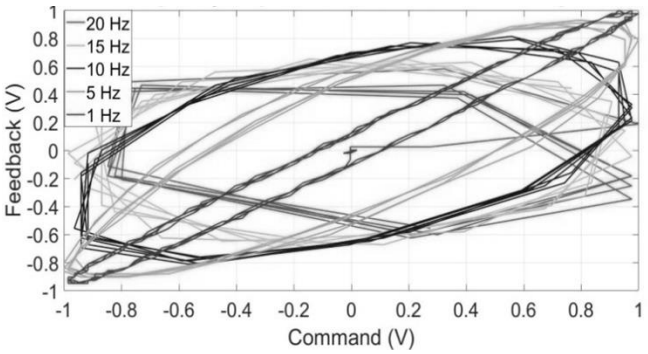

Figure 12: Lissajous figures of experimental data at selected frequencies.

A comparison of the actual test data and calculated from the FRA output is superimposed and shown in Figure 13.

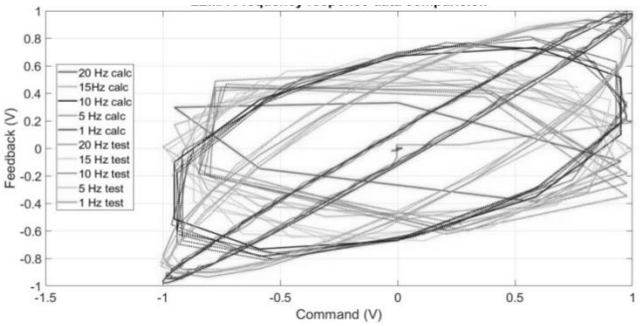

Figure 13: Comparison of Lissajous figures of experimental data and EMA model output data

From the above test and calculated figures, it is evident that the Lissajous figures are able to graphically extract information such as 90º phase and -3 dB gain frequencies without the need for costly equipment, such as a frequency response analyzer, which needs to acquire test data, compare it with standard sinusoids, and arrive at the output

values after the test. The use of Lissajous figures simplifies this process. The 90º phase is directly obtained by the frequency at which the Lissajous figure becomes horizontal, and the-3 dB frequency is the frequency of the Lissajous figure with the minimum aspect ratio.

4. LISSAJOUS FIGURES FOR SYSTEMS HEALTH MONITORING

This section focuses on experimental methods to verify the possibility of using Lissajous figures of the input (command) and output (feedback) of flight actuators from servo controller sensors to arrive at the system's health parameters. Systems health monitoring is another candidate in which large amounts of data is generated and processed to obtain the condition of engineering systems. Systems health monitoring generally uses additional sensor data such as vibration, acoustics, or current data for systems health monitoring techniques such as vibration, acoustics, and MCSA respectively. Generally, data acquisition for such information is performed at high sampling rates on the order of kHz; however, most of the mechanical system health monitoring signatures will be at lower frequencies as they act as low-pass filters. The signals acquired for system health monitoring will have inherent noise; hence, preprocessing is required before analysis. However, in the case of mechanical servo systems, the sensor data is already processed in the servo controller to obtain the desired performance in the feedback loop. Hence, using the same information for systems health monitoring would simplify extracting system health monitoring parameters. In this study, an attempt is made to use readily available position commands and feedback data for system health monitoring of flight actuation servo systems. Information is extracted from the data using Lissajous figures of command and Feedback signals.

Shashikumar and Vijayakumar (2021) used Lissajous curves to analyze the instantaneous voltage and current frequencies of three-phase induction motors to identify four types of lab-induced faults. They compared Lissajous trajectory curves and instant current signature curves to prove the economic resemblance of faults with benchmarks. In this section, we attempt to apply Lissajous figures for health monitoring of electromechanical servo actuators using brushless direct-current motors. They used additional sensors and worked on induction motors, which generally operate at constant speed. This study focuses on the use of a similar technique for servo actuators that generally run at oscillatory commands without using any additional sensors.

4.1. Systems health monitoring tests conducted

Available test data from past experiments performed on a healthy actuator and the same actuator with injected faults is used in the analysis. The experimental setup is explained by Babu et al., (2011), and the experiments specific to this study are listed and abbreviated for use as legends in the plots below.

Tapas (2021) presented the geometry of power flow and harmonic analysis using Lissajous information to improve the performance of power distribution systems. He used Lissajous patterns for health monitoring of power distribution systems and to analyze the harmonics in electric load dispatch. He used Lissajous figures for harmonic analysis and fault diagnosis for linear and nonlinear power distribution systems for electrical loads. Massive simulations were performed to arrive at a power flow method using Lissajous patterns and verified with practical applications. In this study, attempts are made to maximize information by representing the data using Lissajous figures and manipulating them to arrive at simpler system health monitoring tasks.

Experiments were conducted using linear-flight electromechanical actuators. The test data is acquired at 100 Hz (low) for the EMA position command and feedback. Data is also acquired at 2.5 kHz (high) to acquire other parameters, such as motor current and vibration. A healthy actuator is designated as 'h' and is faulty with a fault code, as given below. Initially, the experiment is conducted on a healthy actuator without load application (hol), with a 200 kgf (h2l) load, and 500 kgf load(h5l). A test with high data sampling on a healthy system with a 200 kgf load (h2l) and a healthy system with a 500 kgf load (h5h) was also conducted. The legends in the figures are as given:

Fault code : Systems with induced faults

C20: Clearance 0.2mm in the gear shaft

C40: Clearance 0.4mm in the gear shaft

E20: Eccentricity of 0.2mm in gear shaft

E60: Eccentricity of 0.6mm in gear shaft

G1: Gear with one teeth removed fault

G2: Gear with two teeth removed fault

p: preload in satellite roller screw

The faulty system cases are designated in abbreviations as fault code followed by load in kgf x 100.

Example: G15 is the experiment conducted on EMA with one gear tooth removed and performed at a 500 kgf loading condition.

4.2. Lissajous figures of EMAs with various faults using frequency response test data

Various experiments are conducted for system health monitoring like frequency response, harmonic response, endurance and low-frequency and low-aplitude test. Experimental data of the frequency response tests, represented as Lissajous figures, are discussed in this

section. The effect of the load on the Lissajous figures in both healthy and fault induced experiments are as follows.

4.2.1. Effect of load on Lissajous figure

This section focuses on studying the effect of the load on the Lissajous figures of the frequency response tests. The test is conducted on a healthy actuator without applying any load. The same experiment was repeated at a load of 200 kgf (10% of the designed load).

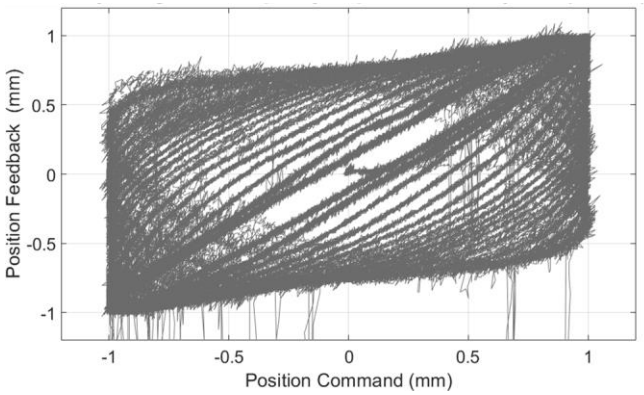

Figure 14: Lissajous figures of frequency response for healthy EMA at no load

Ruijin Wang, Wen Wang, Zhanfeng Chen, Zhiqian Sang, Chuanyong Wang, Keqing Lu, Fuming Han and Bingfeng Ju, (2022) discussed the similarities and differences between the Lissajous curve and dynamic hysteresis of piezoelectric actuators using the Proposed Lissajous curve Prandtl-Ishlinskii model. The proposed model is based on the Lissajous curve to describe and compensate for dynamic hysteresis in piezoelectric actuators. Lissajous figure better represents the dynamic hysteresis, and load effects can be extracted even in such small displacement piezoelectric actuators. The same is experimented with to servo actuators with relatively large displacements.

Lissajous figures of the frequency response tests performed on a healthy EMA run under the no-load condition are shown in Figure 14, and those at a 200 kgf load are shown in Figure 15. The Lissajous figures for both the cases look similar. This reiterates the fact that the load within the design limits has a minimal effect on the condition monitoring parameters, as concluded by the motor current signature analysis (MCSA) by Babu et al., (2011). Even full load tests at 1500 kgf also didn't show appreciable variation in MCSA. However, further careful observation of the Lissajous figures for 200 kgf case itself reveals identifiable change. In the Lissajous figure representing the loaded case, The high-frequency loops rotation angle of the Lissajous figure is observed to be relatively more. The aspect ratio also is found to be relatively wider when compared with the no-load case Lissajous figure.

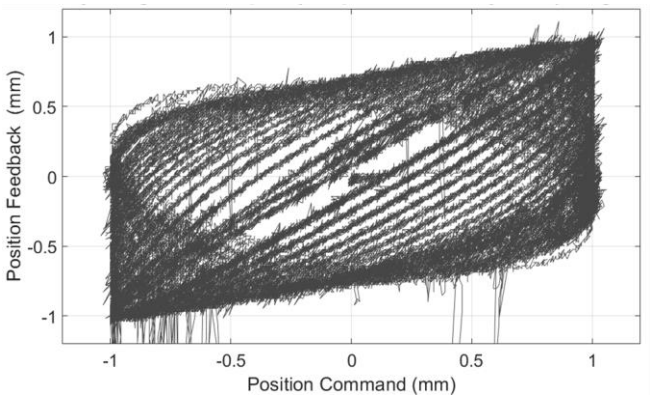

Figure 15: Lissajous figure of frequency response of healthy EMA at 200 kgf load

4.2.2. Effect of gear fault on Lissajous figure

A change in the Lissajous figure of the EMA with one tooth removed gear fault (G1) is observed when compared with the healthy EMA data plotted in Figure 16. Lissajous figure shape changed significantly in the top left and bottom right corners. Smoothening is observed in the curvature. The Lissajous figures representing high frequencies have inflated (lower aspect ratio) when compared to the Lissajous figures representing healthy actuator tested at no-load and 200 kgf load, as shown in earlier Figure 14 and Figure 15 respectively.

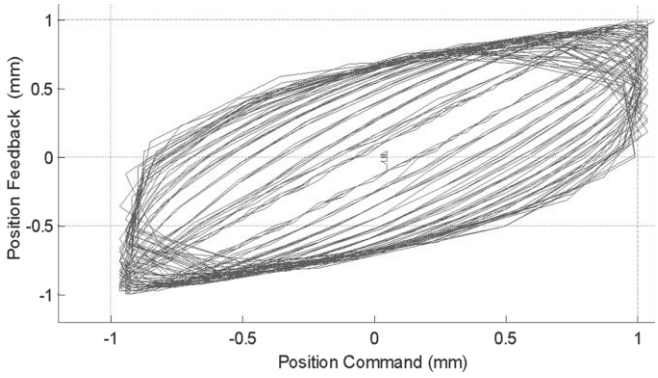

Figure 16: Lissajous figure of frequency response of EMA with gear 1 fault

The gear fault smears the Lissajous figure at the top-left and bottom-right corners, representing a greater change in the phase lag. The phase lag increased from loops representing low frequency of 1 Hz to loops representing a high frequency of 20 Hz. Hence, the width of the Lissajous figure is found to increase with an increase in the input frequency owing to the phase lag, deviating in the direction normal to the x=y line, which represents the ideal system. The gear fault induced can easily be identified by the change in the shape of the Lissajous figure. It is more convenient to use this type of graphical information to train expert systems for classification problems of this type of fault.

4.3. Lissajous figures of EMAs with various faults using simpler tests

Frequency response tests are difficult to conduct and require expensive frequency response analyzers and a sturdy test bench as the EMA rattles during the test, particularly during high-frequency commands. Moreover, the test data are in the time domain, and to arrive at the test outcome, transforming data into the frequency domain is necessary.

In this section, an attempt is made to arrive at the system health monitoring information of flight actuators using relatively simpler tests, routinely performed on flight servo actuators. The methodology used to represent the test data using Lissajous figures is arrived at. Further transformation of the Lissajous figures to simplify the extraction of the system's health parameters from the test data is attempted. The Lissajous figure is rotated by 45º to amplify the information in the test data. In addition, the figures are spiralled out by dot multiplication with the time vector, enabling the extraction of the temporal information (time instant of the anomaly). The actual position of the fault with respect to the stroke of the actuator could be identified from transformed Lissajous figures unlike in direct figures.

Experiments were conducted with various inputs to the healthy system and the system with various faults induced, as listed in Section 4.1. Typical plots of the Lissajous figures for various inputs to the EMA are shown in Figure 17. Lissajous figures of EMA response to sinusoidal command (a), Frequency response test with a 1V command, with frequency changing from 20 Hz to 1 Hz in intervals of 1 Hz, dwelling two cycles at each frequency (b), High-amplitude & low-frequency command (c), low-amplitude & low-frequency command (d), and constant velocity (ramp) command (e).

Figure 17 (a) shows the Lissajous figure of the healthy actuator test data overlapped with the Lissajous figures representing the test data of the faulty actuators with various induced faults. Not much information can be extracted directly in the case of a system response to a sinusoidal command. Figure 17 (b) shows the Lissajous figures of the frequency-response data of the actuators with and without faults. It is clear from the figure that the faults induced in the actuator caused appreciable changes in the Lissajous figures. The Lissajous figures in Figure 17 (c) represent the actuator commanded with high-amplitude low-frequency responses under healthy and fault-induced conditions. It depicted feedback following the input by the system and no observable changes in Lissajous figures corresponding to healthy and fault-induced actuators is noted. Figure 17 (d) shows the Lissajous figures of the low-amplitude low-frequency test data, which were obtained at very low speeds with minimal inertial effects. The test covers the miniscule portion of the stroke at very low speed; hence, it is useful for determining the non-linearities in the actuator. The width of the flat line near zero represents the threshold value, and the width of the flat portions at extremes (change in direction) represents backlash, resulting in a direct understanding of the non-linearities of the system. The Lissajous figures representing the experiments vary and are found to be useful in arriving at actuator system health monitoring parameters. Figure 17 (e) shows the response of the system to a constant velocity input, which is the closest condition to stationary operation, as the electric motor in the actuator runs at a constant speed for most of the test duration. Here, the Lissajous figures have identifiable changes that represent the health condition of the actuator. Further data analysis is required to obtain necessary information.

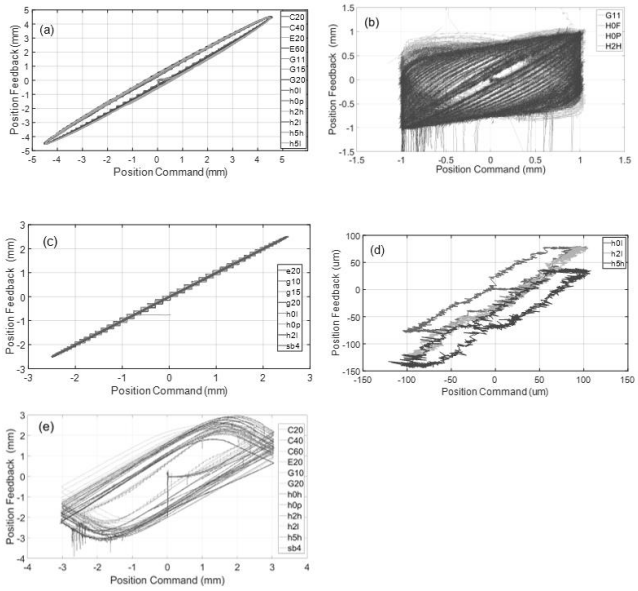

Figure 17: Typical plots of Lissajous figures for Sinusoidal input (a), Frequency response (b), High-amplitude & low-frequency (c), Low-amplitude & low-frequency (d) and Ramp (e) tests

4.3.1. Transformation of data to maximise information in Lissajous figures by rotating and spiralling

The ideal Lissajous figure is a straight line with a slope of 45º, as the output of the actuator is expected to follow the input, with an amplitude ratio of 1 (slope) and zero phase lag (the expected width of the figure is zero). To maximize information visibility, the figure can be viewed from a direction perpendicular to the data spread, similar to the principal axis (minimum entropy). In the case of the Lissajous plot, the abscissa was 45º. Hence, the Lissajous figure rotated by 45º to improve the extraction of information analogous to the residual plot of the mathematical fit to test data.

Generally, in the Lissajous figure representing the test data, each cycle of the actuator forms one loop, and all such loops overlap owing to the reciprocating action of the actuator,

resulting in a stable Lissajous figure. However, owing to the changes in the system parameters and external load disturbances, the Lissajous loop deviates from the standard Lissajous figure. It will be difficult to identify from which cycle this deviation is initiated as Lissajous loops representing all cycles overlap. Hence, spiraling out the data is attempted to retain the temporal information to correlate the actuator cycle with the Lissajous loop. In addition, within the loops, the spatial information can be obtained from the ordinate, which can be transformed into the actuator output shaft position (stroke). To arrive at the instance of failure and the location of the stroke at which such deviation occurred, the Lissajous figure was spiraled out to enable identification of the cycle in which an anomaly is observed or the start of a gradual deviation. The spiraling is done by the dot product of actuator position data with instantaneous time, and then plotting the Lissajous figure. MATLAB (2019a) code is used for the analysis.

Method adopted: The Lissajous figures of the actuator response to a typical sinusoidal command for various fault cases are shown in Figure 18. All plots appear similar, making differentiating fault signatures impossible by simple observation. Only the two gear teeth removed (g) and the preloaded roller screw faults (i) were only distinguishable in direct Lissajous figures. All the other cases had similar Lissajous figures. In addition, the Lissajous figures representing both the gear tooth removed fault (g) and preloaded roller screw fault (i) were also similar and not separable. Hence, various faults cannot be differentiated by directly observing Lissajous figures.

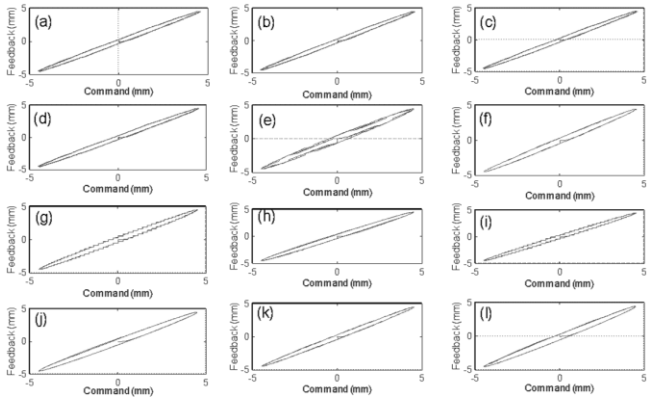

Figure 18: Lissajous figures of healthy system and various faults induced system for sinusoidal input (a) C20,(b)C40, (c) E20, (d) E60, (e) G11, (f) G15, (g) G20, (h) hol, (i) hop, (j) h2h, (k) h2l, (l) h5h

The above Lissajous figures in Figure 18 are rotated by 45^o and are shown in Figure 19 to view them in the maximum information direction. Rotated Lissajous figures improved the visibility of the test data and made the fault cases easily distinguishable. The clearance (a,b), eccentricity (c,d), preload (i), and gear faults (e,f,g) are separable. The load effects are distinguished by the spread of the figure during the initial kink suppression with an increase in load (h,k, and l). In the case of no load (h), the initial kink is greater; at a 200 kgf load (k), a small kink is visible, and at 500 kgf, the kink is almost absent. The Lissajous figures of clearance (a,b) and eccentricity faults (c,d) are similar, making them difficult to distinguish. Gear faults are more clearly visible in no-load conditions with wider bands (e,g), and the figure with loading the actuator with gear fault (f) reduced this band but was clearly distinguishable from the other cases. The Lissajous figures representing the gear tooth fault (g) and preload of the roller screw (i) are also similar. This study concludes that the Lissajous figures are sensitive to faults. Their variations for different faults can be identified through observation by experience. The same can be used for the supervised training of expert systems and mapping of changes in Lissajous figures for fault classification.

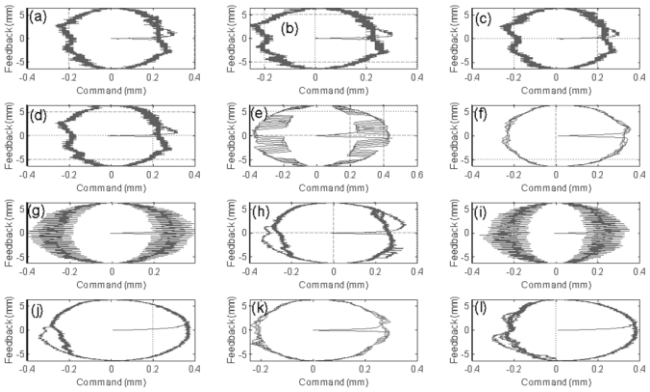

Figure 19: Rotated Lissajous figures of healthy system and faults induced system for sinusoidal input (a) C20, (b) C40, (c) E20, (d) E60, (e) G11, (f) G15, (g) G20, (h) hol, (i) hop, (j) h2h, (k) h2l, (l) h5h

Lissajous figures are good at extracting deviations owing to abrupt changes in the figures. However, in the case of actuators, The Lissajous figures overlap for all cycles of operation, resulting in the loss of temporal information. To retain temporal information, the rotated data are multiplied with the instantaneous time to spiral out the plot, thereby retaining the temporal information. The classification becomes easier and enables the extraction of additional information by pinpointing the instant of deviation due to a fault at a particular stroke of EMA or time instant. In Figure 20, each loop covers one full stroke of the actuator, and each loop represents the Lissajous figure for the corresponding cycle (stroke). This method augments additional temporal information by retaining condition monitoring information, as shown in Figure 19. The forward stroke of the EMA is represented by the right-half plane portion of each loop, and the return stroke of the EMA is represented by the left-half plane. Sazali Yaacob, Amir Rasyadan and Pranesh Krishnan, (2021) presented simulation analysis methods to minimize the load and speed variations of induction motors in the detection and localization of drive faults using Lissajous patterns of the phase-current trajectory. The

variation in the Lissajous pattern between healthy and faulty switch operations is used to localize faulty switches. They experimentally verified that the transient current condition during load and frequency changes did not affect fault detection. The Lissajous figure was smoothly spiraled from zero load to maximum load operation to take advantage.

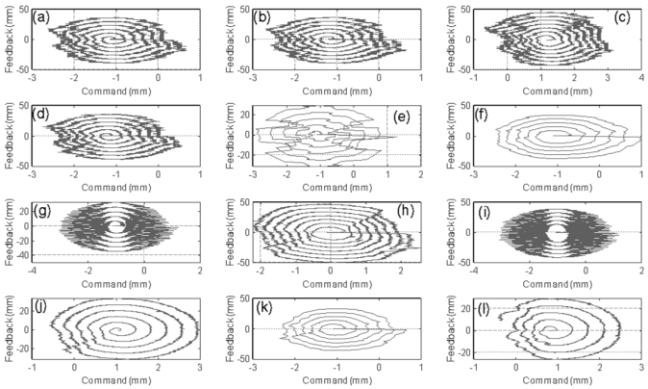

Figure 20: Rotated and spiraled Lissajous figures of healthy system and faults induced system for sinusoidal input (a) C20, (b) C40, (c) E20, (d) E60, (e) G11, (f) G15, (g) G20, (h) hol, (i) hop, (j) h2h, (k) h2l, (l) h5h

The experimental data is represented by overlapping Lissajous patterns and attempted to retain temporal information of events with huge effects on actuators, such as instantaneous overload, jamming of roller screws, and foreign particle inclusions. The test data represented in Figure 19 as Lissajous figures are spiraled and shown in Figure 20, separating each cycle of EMA and making it clearly visible in the figures. The Lissajous figures can be attributed to the EMA position and operating cycle. Lissajous figures can be treated as polar plots. Each loop represents one cycle of EMA operation, starting from the innermost loop. The developed technique is applied to Lissajous figures of constant velocity (ramp) test data. The plots depict more condition monitoring information with relative ease, as shown in Figure 21.

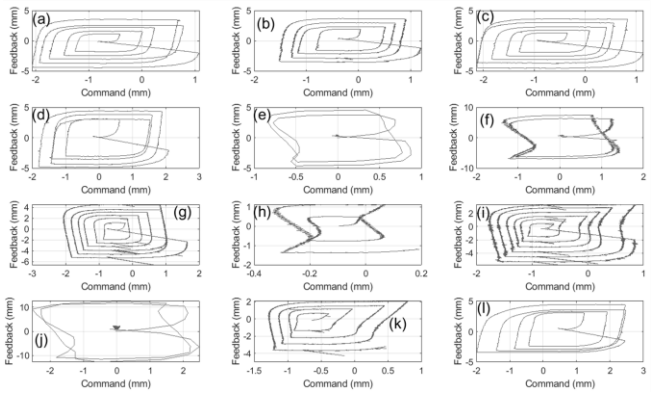

Figure 21: Rotated and spiraled Lissajous figures of healthy and faults induced system for ramp input(a) C20, (b) C40, (c) E20, (d) E60, (e) G11, (f) G15, (g) G20, (h) hol, (i) hop, (j) h2h, (k) h2l, (l) h5h

The clearance errors (a,b) are manifested as non-overlapping Lissajous curves. Increase in clearance from 0.2 mm (a) to 0.4 mm (b) resulted in added noise in the Lissajous curve. Eccentricity fault (c,d) resulted in overlapping Lissajous, with minimal overlap for 0.3 mm eccentricity (c) to a large overlap for 0.6 mm eccentricity fault case. The Gear1 fault (e,f) is manifested in the complete warping of the Lissajous figure along the abscissa. The warpage increased from 100 kgf loading (e) to 200 kgf loading (f). The load increased from no load to 500 kgf (i,k,. l) resulted in a shape change in the Lissajous curve representing positive stroke, contraction of the positive half, and expansion of the negative half. The Lissajous figure representing Gear2 fault (g) is completely different from the Gear 1 fault figures (e,f). The load of the roller screw manifested as a huge warpage of the Lissajous figure (h), similar to the gear 1 fault loading case, making it difficult to separate.

5. CONCLUSIONS

The inherent advantage of non-verbal representation of actuation systems acceptance and health data can aid engineers with easier decision making for flight worthiness. The Lissajous patterns representation is found to be beneficial as no additional sensors are needed for servo actuators, where the input and output position data are available. Lissajous patterns are found to be useful in extracting the information necessary for flight actuator acceptance tests, easing repetitive tasks of quality engineers, and develop image processing based expert systems to handle large amounts of data. Lissajous patterns can provide a quick view of the outcomes of tests such as pass fail criterion and also can extract parameters in complex tests such as frequency response in depicting actuator bandwidth information.. Lissajous figures are also found to be helpful in a simple representation of the system health monitoring information of flight servo actuators directly in some cases. Transformations of Lissajous figures, such as rotation and spiraling are found to be useful in extracting additional temporal health monitoring information with ease.

Graphical representation of test data and test outcome repositories are needed to develop expert systems taking advantage of recent research in classification algorithms. Standardization of graphical methods and comparison studies with standard methods are needed for extending the advantage of the current classification algorithms for flight actuators testing.

REFERENCES

Albert F K, (1980). Direct Integration of transient rotor dynamics, *AVRADCOM technical Report* 79-42, Technical paper no 1597, NASA.

Armughan H., Sufi T.G. & Abdul Q.K., (2016). *A Park's Vector Approach Using Process Monitoring Statistics of Principal Component Analysis for Machine Fault Detection*, 978-1-5090-3552-6/16 IEEE.

Avoci M.U., Carratu M., Pietrosanto A., Paciello V. & Lay-Ekuakille V., (2020). *Vibrations Measurement and Current Signatures for Fault Detection in Asynchronous Motor*, 978-1-7281-4460-3/20 IEEE.

Babu G.S, Lingamurthy A & Sekhar A.S, (2011). Condition monitoring of brushless DC motor-based electromechanical linear actuators using motor current signature analysis, *The International Journal of Condition Monitoring*, Volume 1, Issue 1, pg 20-32.

Bhaskar M.R., Asish D., Babu G.S., Venugopal D, & Chattopadhyay A.K., (2015). Development of Electrical Actuation System for Thrust Vector Control, 9th *National Symposium and Exhibition on Aerospace and Related Mechanisms*, ARMS-2015-135.

Chenguo Y., Zhongyong Z., Yan M., Chengxiang L., Yifan L. & Guochao Q., (2015). Improved Online Monitoring Method for Transformer Winding Deformations Based on the Lissajous Graphical Analysis of Voltage and Current, *IEEE Transactions On Power Delivery*, Vol. 30, No. 4. doi:10.1109/TPWRD.2015.2418344.

Gurevich I.B, Yashina V.V and Ablameyko S.V (2018). Development and Experimental Investigation of Mathematical Methods for Automating the Diagnostics and Analysis of Ophthalmological Images. *Pattern Recognit. Image Anal*. 28, 612–636 doi:10.1134/S1054661818040120.

Hisham A.H, Al-Khazali, & Mohamad R.A, (2012). Geometrical and graphical representations analysis of Lissajous figures in rotor dynamic system, *IOSR Journal of engineering*, Vol 2(5) pp:971-978.

Qing Bi, Dingguo S., Jian L., (2019). Signal Correction of Linear Hall for PMSM Control System, *IEEE 3rd Advanced Information Management, Communicates, Electronic and Automation Control Conference* (IMCEC), 978-1-7281-0513-0/19.

Ruijin W., Wen W., Zhanfeng C., Zhiqian S., Chuanyong W., Keqing L., Fuming H. & Bingfeng J., (2022). Modeling and compensation for dynamic hysteresis of piezoelectric actuators based on Lissajous Curve. *Sensors and Actuators*. Vol. 335, 113353, https://doi.org/10.1016/j.sna.2021.113353.

Sazali Y., Amir R. & Pranesh K., (2021). Simulation Analysis for Induction Motor Drive Fault Detection and Localization Under Variable Load and Speed Operation, *International Scientific Forum (ISF), IOP Conf. Series: Materials Science and Engineering*, doi:10.1088/1757-899X/1127/1/012024.

Shashikumar K. & Vijayakumar V., (2021). *Detecting industrial motor faults with current signatures*. PMID: 36398279; PMCID: PMC9634139. doi: 10.12688/f1000research.54266.1.

Tapas H, (2021). A geometry of the power flow and harmonic analysis with the Lissajous figures, *International conference on sustainable energy and future electric transportation* (SeFeT).

Urala B.K., Rathin R.N, Srirangaraj S., Aparajita D., Scott B., Venu G. & Krishna R., (2018). Automated Extraction of Data from Binary Phase Diagrams for Discovery of Metallic Glasses. In: Fornés, A., Lamiroy, B. (eds) *Graphics Recognition. Current Trends and Evolutions. GREC. Lecture Notes in Computer Science*, vol 11009. Springer, Cham. doi:10.1007/978-3-030-02284-6_1

Xiaowen L & Juncheng L, (2021). Research on the Application of Machine Learning Technology in the Automatic Recognition System of Engineering Graphics, *IEEE 3rd International Conference on Civil Aviation Safety and Information Technology* 716-720, doi:10.1109/ICCASIT53235.2021.9633603.

Sreedhar Babu Gollapudi is presently working as Scientist 'F' in Control Systems Laboratory of Research Centre Imarat, DRDO, Hyderabad. Concurrently pursuing PhD in IIT Madras in the area of condition monitoring of Flight actuation systems. He is working in the area of flight control actuation systems from 20 years. He is expert in realisatin, performance evaluation and testing of electro mechanical actuation systems for aerospace applications.

Prof. Seshadri Sekhar A is currently Director, IIT Palakkad, India. He worked as Professor in Machine Design Section Indian Institute of Technology Madras, Chennai. In addition to vast teaching experience in the area of machine dynamics his research interests include Condition Monitoring, Rotor dynamics, Vibration engineering, Product Design, Tribology, Engineering optimization and FEM Analysis.

Dr Lingamurthy is an emeritus Scientist with 33 years of experience in Aerospace actuation systems. His areas of expertise includes Electro pneumatic, electro mechanical actuation systems, Micro electro mechanical systems, design, development & realization of avionics systems and sensors.